Journal of Magnetic Resonance **146,** 196–203 (2000)
doi:10.1006/jmre.2000.2139, available online at http://www.idealibrary.com on IDEAL®

Two-Dimensional Pulsed TRIPLE at 95 GHz

B. Epel[1] and D. Goldfarb

Department of Chemical Physics, Weizmann Institute of Science, Rehovot 76100, Israel

Received March 17, 2000; revised June 6, 2000

The one-dimensional (1D) pulsed TRIPLE resonance experiment, introduced by Mehring *et al.* (M. Mehring, P. Höfer, and A. Grupp, *Ber. Bunseges. Phys. Chem.* 91, 1132–1137 (1987)) is a modification of the standard Davies ENDOR experiment where an additional RF π-pulse is applied during the mixing time. While the first RF pulse is set to one of the ENDOR transitions, the frequency of the second RF pulse is scanned to generate the TRIPLE spectrum. The difference between this spectrum and the ENDOR spectrum yields the difference TRIPLE spectrum, which exhibits only ENDOR lines that belong to the same M_S manifold as the one selected by the first RF pulse. We have extended this experiment in two dimensions (2D) by sweeping the frequencies of both RF pulses. This experiment is particularly useful when the spectrum is congested and consists of signals originating from different paramagnetic centers. The connectivities between the peaks in the 2D spectrum enable a straightforward assignment of the signals to their respective centers and M_S manifolds, thus providing the relative signs of hyperfine couplings. Carrying out the experiment at high fields has the additional advantage that nuclei with different nuclear gyromagnetic ratios are well separated. This is particularly true for protons which appear at significantly higher frequencies than other nuclei. The feasibility and effectiveness of the experiment is demonstrated at W-band (94.9 GHz) on a crystal of Cu^{2+}-doped L-histidine. Homonuclear ^1H–^1H, $^{14}N/^{35}Cl$–$^{14}N/^{35}Cl$ and heteronuclear ^1H–$^{14}N/^{35}Cl$ 2D TRIPLE spectra were measured and from the various connectivities in the 2D map the ^1H, ^{14}N, and ^{35}Cl signals that belong to two different Cu^{2+} centers were identified and grouped according to their M_S manifolds.

Key Words: **high field pulsed EPR; ENDOR; TRIPLE.**

INTRODUCTION

The rapid development of high field EPR in the past few years resulted in an increasing number of applications which clearly show the advantages and the new possibilities it offers (*1–3*). It is only natural that the developments in high field EPR paved the way for high field electron-nuclear double resonance (ENDOR) and the construction of several pulsed ENDOR spectrometers operating at 95 GHz (W-band) (*4–6*) and 140 GHz (D-band) (*7*) have been described. Although the number of the reported high-field ENDOR applications is still small, the advantages are clear. Due to the significantly larger nuclear Zeeman interaction, ENDOR signals from different nuclei are better resolved and nuclei with low gyromagnetic ratios can be observed also when the hyperfine interactions are small (*8–10*). For example, the notorious overlap between strongly coupled ^{14}N and weakly coupled ^1H (*11*), which often prevents the application of proton ENDOR for structural studies at X-band, does not exist at high frequencies. Furthermore, ^2H ENDOR becomes less problematic, compared with X-band, because the signals appear at significantly higher frequencies, around 20 MHz, which is much more convenient experimentally (*12*). The wider spread of powder patterns governed by small g-anisotropies allows orientation selective ENDOR experiments (*13, 14*). In high spin systems, high order effects that increase inhomogeneous broadening are significantly reduced, improving the resolution of the EPR spectrum and thereby facilitating ENDOR measurements (*15*). Finally, the large thermal polarization achieved at high magnetic fields and low temperatures allows straight forward determination of the signs of the hyperfine couplings and the zero field splitting (ZFS) (*10, 15, 16*).

We have shown that routine low temperature (4–5 K) W-band ^1H and ^2H pulsed ENDOR measurements of paramagnetic transition metal sites in a variety of systems such as frozen solutions and single crystals of metalloproteins, transition metal substituted molecular sieves, and encapsulated complexes in zeolites, are possible (*6, 15, 17, 18*). Although the frequency range of many different types of nuclei are well apart at W-band, we still face the problem of congested spectra, especially for protons. The congestion is due to overlapping signals arising from different protons, different EPR transitions (in the case of $S > \frac{1}{2}$ system) and/or different EPR centers (*15*). One approach to simplify spectra and assign signals is isotopic labeling. This, however, is not always simple and requires considerable synthetic efforts. It is, therefore, necessary to develop experiments that will enhance resolution and facilitate signal assignment.

Two-dimensional (2D) spectroscopy is a significant advance in this direction since it provides spectral correlations, and enhanced resolution due to the spread of the spectrum into a second dimension. An excellent example is the 2D hyperfine sublevel correlation (HYSCORE) experiment (*19*), which has revolutionized the field of electron-spin echo envelope modu-

[1] On leave from MRS Laboratory, Kazan State University, Kazan, 420008, Russian Federation.

1090-7807/00 $35.00

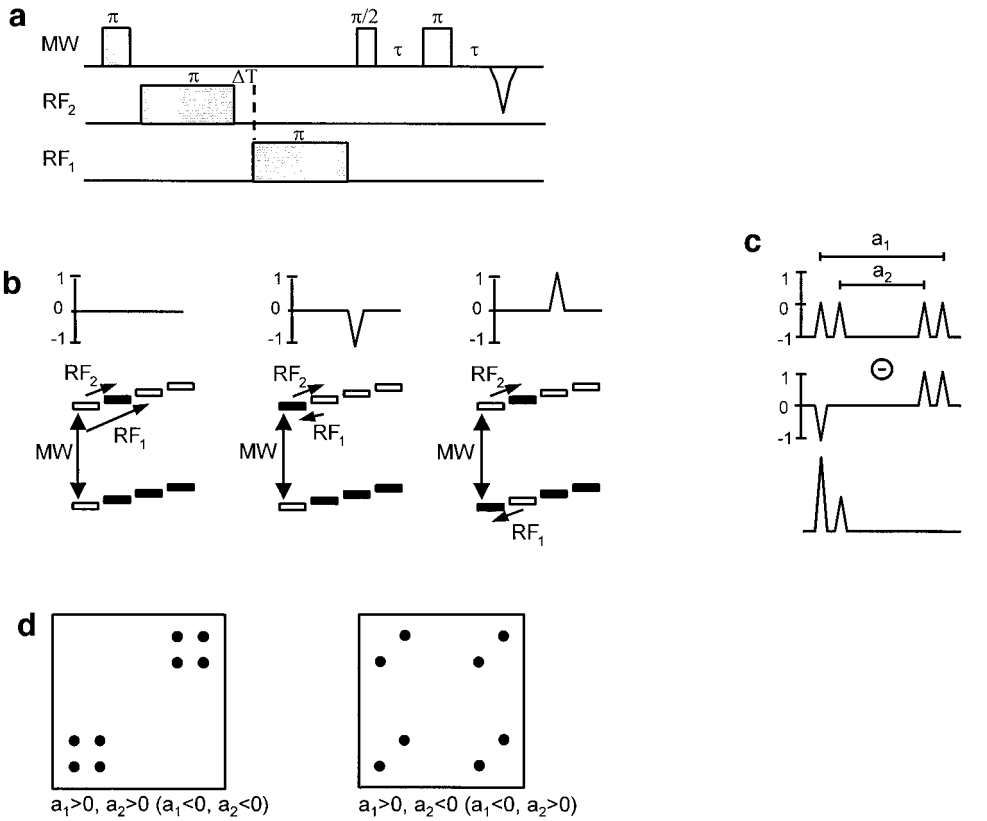

FIG. 1. (a) The pulse sequence of the TRIPLE experiment. (b) Energy-level diagram for a $S = \frac{1}{2}$ coupled to I_1, $I_2 = \frac{1}{2}$ with hyperfine couplings of a_1 and a_2, where $\nu_I > a_1, a_2 > 0$. The first, second, and third diagrams show the evolution of the energy levels population during the TRIPLE experiment when $RF_1 = RF_2$, RF_1 and RF_2 affect nuclear transitions in the same M_S manifold, and different manifolds, respectively. (c) ENDOR spectrum (top), TRIPLE spectrum (middle) and difference TRIPLE spectrum (bottom) for RF_2 set to the lowest frequency peak in the ENDOR spectrum. (d) 2D difference TRIPLE spectra for $a_1 > 0$, $a_2 > 0$ and $a_1 > 0$, $a_2 < 0$.

lation (ESEEM) spectroscopy. In this experiment correlations between nuclear frequencies belonging to different M_S manifolds of the same paramagnetic center are obtained. Another example is the complementary 2D DONUT-HYSCORE experiment which provides nuclear frequencies correlations within a particular M_S manifold (*20*). A 2D experiment that combines time domain ENDOR and the electron-spin echo envelope modulation (ESEEM) phenomenon is the chirp ENDOR-HYSCORE experiment which provides correlations of nuclear frequencies belonging to different M_S manifolds (*21*). This experiment is advantageous in the case where nuclear transitions are easily excited, and for spin systems with weak forbidden EPR transitions. The HYEND (Hyperfine-correlated electron-nuclear double resonance) experiment is another example of a 2D experiment that correlates the hyperfine splittings with the ENDOR frequencies (*22*). The two last experiments require the application of nonselective microwave π pulses, which is somewhat problematic with current state of the art high field ENDOR spectrometers due to their limited microwave power. Another recent example is the ENDOR-ESEEM correlation experiment (*23*). In ENDOR spectroscopy, correlations between signals belonging to the same paramagnetic center and the same M_S manifold can be obtained by extending the 1D pulsed TRIPLE experiment into two-dimensions, as introduced in the present work.

The TRIPLE experiment (also referred to as double ENDOR) was first designed in the continuous mode (CW) for determining relative signs of hyperfine coupling constants (*24*). It was initially applied to solid samples and then to liquids (*25*). The pulse mode analog of the TRIPLE experiment, shown in Fig. 1a, was reported by Mehring and coworkers (*26*). The Mims-TRIPLE variant of the experiment has been applied at X-band for the assignment of exchangeable ^2H in $[3Fe–4S]^+$ clusters (*27*). Another example of a TRIPLE application is the investigation of the heterogeneity and nuclear longitudinal relaxation rates of radicals in polymers (*28*).

The mechanism of the experiment is illustrated in Fig. 1b on a simple system of one electron spin, $S = \frac{1}{2}$, coupled to two nuclei, I_1, $I_2 = \frac{1}{2}$ with hyperfine couplings a_1 and a_2, where $\nu_I > a_1 > a_2 > 0$. The ENDOR spectrum of such a system (Fig. 1c, top) consists of two doublets, centered at the nuclear Larmor frequency ν_I, with splittings of a_1 and a_2. The first microwave (MW) π-pulse selectively inverts the populations of one of the EPR transitions and the application of the MW

$\pi/2$-π-detection sequence after a time T generates an echo with a negative polarity. The application of a RF_2 π-pulse, on resonance with one of the ENDOR transitions in the $M_S = \frac{1}{2}$ manifold, inverts the populations in the corresponding NMR transition (Fig. 1b, left). This equalizes the populations of the energy levels of the EPR transition selected by the MW π pulse and results in a zero intensity echo. A second RF π-pulse with a frequency RF_1 alters the echo intensity when (i) RF_1 is on resonance with any other ENDOR transitions in the other manifold, $M_S = -\frac{1}{2}$, that has a common energy level with the selected EPR transition (see Fig. 1b, right), or (ii) RF_1 is on resonance with the ENDOR transition selected by the first RF pulse, i.e., $RF_1 = RF_2$ (Fig. 1b, middle). In case (i) the echo intensity will change from "zero" to a positive echo, whereas in (ii) a negative echo will be generated. Sweeping the frequency of the RF_1 pulse produces the TRIPLE spectrum shown in Fig. 1c (middle). Subtraction of the TRIPLE spectrum from the normal ENDOR spectrum produces the difference TRIPLE spectrum, which shows only the ENDOR lines that belong to the same M_S manifold as that selected by the RF_2 pulse (Fig. 1c, bottom). In the 2D TRIPLE experiment both RF_1 and RF_2 are swept. The 2D difference TRIPLE spectra for the cases a_1, $a_2 > 0$ (a_1, $a_2 < 0$) and $a_1 > 0$, $a_2 < 0$ ($a_1 < 0$, $a_2 > 0$) are presented in Fig. 1d.

In this work we present W-band 2D TRIPLE measurements which demonstrate the feasibility and effectiveness of the experiment. The measurements were carried out on a crystal of Cu^{2+} doped L-histidine HCl · H_2O (Cu–His). The space group of the crystal is $P2_12_12_1$ and two Cu^{2+} ions, located in two different, symmetry related, crystallographic sites contribute to the EPR and ENDOR spectra (*29*). This system has been a subject of many investigations and the hyperfine and quadrupole tensors of the coupled nuclei have been determined (*29*, *30*). The Cu^{2+} ions are coordinated by two histidine molecules through their amino and imidazole nitrogens, respectively. In addition, it is coordinated to a third histidine molecule through its carboxylic oxygen, and to a water molecule and two chloride ions. This coordination structure leads to a congested and complicated ENDOR spectrum as it consists of lines arising from two strongly coupled ^{14}N nuclei (amino and imino), a number of protons and ^{35}Cl nuclei. The 2D difference TRIPLE spectra provided both homonuclear, ^1H–^1H and ^{14}N/^{35}Cl–^{14}N/^{35}Cl, and heteronuclear ^1H–^{14}N/^{35}Cl correlations from which ^1H, ^{14}N and ^{35}Cl signals belonging to two Cu^{2+} centers were resolved and identified, and the relative signs of their hyperfine couplings were determined.

EXPERIMENTAL

Sample Preparation

0.5% mol $CuCl_2$ were added to an aqueous D_2O solution of 98% L-histidine HCl · H_2O (*31*). Slow evaporation at room temperature over a period of a few days generated crystals. The sample that was used for the measurements was not a single crystal but contained a few fused crystals with slightly different orientations of their crystallographic axes.

Spectroscopic Measurements

Pulsed ENDOR and TRIPLE measurements were performed at W-band (94.9 MHz) on a home built spectrometer (*6*) at 5 K. The ENDOR probehead was similar to that described earlier (*6*) with the exception of a new RF coil (saddle coil with $2 \cdot 10$ turns instead of $2 \cdot 4$) optimized for measurements in 5–40 MHz frequency range and with a reasonable RF field, B_2, for ^1H frequencies (135–155 MHz). With full power of the RF amplifier (3kW pulse) and a unmatched RF circuit with a 50 Ω termination, typical durations of RF π-pulses were 23 μs for ^{14}N/^{35}Cl (at 24 MHz) and 25 μs for ^1H (at 140 MHz), as determined from Rabi oscillations of the corresponding ENDOR lines in the Cu–His spectrum.

All reported experiments were carried out with MW $\pi/2$ and π pulses, $t_{MW,\pi/2}$ and $t_{MW,\pi}$, of 0.1 and 0.2 μs, respectively, τ delays of 0.35 μs and repetition rates of 142 Hz. The field-sweep echo-detected (FS-ED) EPR spectrum was recorded using the two-pulse echo sequence and a magnetic field sweep rate of 0.0016 Ts^{-1}. The RF pulse length in the Davies–ENDOR and TRIPLE experiments was optimized according to the nucleus of interest. In 1D ^1H ENDOR experiments 601 points were sampled with an RF increment, ΔRF, of 0.022 MHz and 1D ^{14}N/^{35}Cl ENDOR spectra were recorded with ΔRF = 0.035 MHz and 251 points. Two-dimensional data sets had 301 points in the ^1H frequency domain and 201 points in ^{14}N/^{35}Cl domain with ΔRF = 0.044 MHz and ΔRF = 0.035 MHz, respectively. The delay, ΔT, between the two RF pulses was 1 μs. For each point in the 2D experiment 3 shots were averaged.

Data Manipulation

Two-dimensional difference TRIPLE data were treated using the Bruker WINEPR software. Baseline correction was carried out for each slice in both dimensions. This procedure is equivalent to the subtraction of the ENDOR spectrum (since the TRIPLE spectrum obtained by sweeping RF_2 with RF_1 off-resonance is equivalent to the normal ENDOR) and yields the inverted difference TRIPLE spectrum. The final step was multiplication by -1 to obtain positive signals, as shown in Fig. 1c.

Simulations

A computer program was designed to simulate ENDOR and 2D TRIPLE experiments. Since the purpose of the present work is to demonstrate the method, we considered the simplest case, an electron spin, $S = \frac{1}{2}$ coupled to n nuclei (protons) with spin $I = \frac{1}{2}$. The first-order ENDOR frequencies, ν_{α_1},

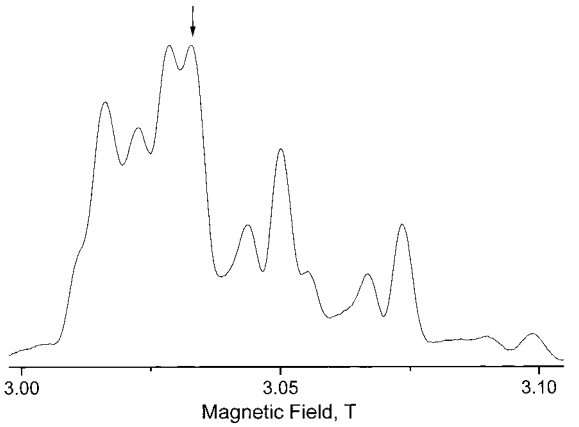

FIG. 2. The W-band FS-ED EPR spectrum of a Cu–His crystal placed at an arbitrary orientation ($t_{MW} = 0.1/0.2$ μs, $\tau = 0.35$ μs, $T = 5$ K). The arrow marks the magnetic field at which ENDOR and TRIPLE experiments were performed.

$\nu_{\alpha_2} \ldots \nu_{\alpha_n}$, ν_{β_1}, $\nu_{\beta_2} \ldots \nu_{\beta_n}$, in the $M_S = \pm\frac{1}{2}$ manifolds, denoted by α and β, are (*32*)

$$\nu_{\alpha,i} = \left| -\nu_I + \frac{a_i}{2} \right|, \quad \nu_{\beta,i} = \left| -\nu_I - \frac{a_i}{2} \right|, \qquad [1]$$

where ν_I is the nuclear Larmor frequency and a_i is the hyperfine splitting of nucleus i. Cross peaks in the 2D difference TRIPLE spectrum appear at $(\nu_{\alpha_i}, \nu_{\alpha_j})$ and $(\nu_{\beta_i}, \nu_{\beta_j})$, where the indices i and j assume all possible values between 1 to n. The cross peak pattern is symmetric with respect to the exchange of the i and j indices and, in principle, it is sufficient to measure only a half of the spectrum. Nevertheless in some cases, for the sake of completeness, we measured the whole spectrum.

RESULTS

The EPR spectrum of a single crystal of Cu–His should exhibits two quartets, corresponding to the two crystallographic sites (*30*). The FS-ED EPR spectrum of the Cu–His crystal we used, placed at an arbitrary orientation with respect to the magnetic field, is presented in Fig. 2. It exhibits more than 8 lines, thus indicating that the sample is not a single crystal but contains one or two additional crystals. The ENDOR and TRIPLE measurements were carried out at 3.0335 T, where signals of at least two different Cu^{2+} centers overleap. The ^{1}H Davies ENDOR spectrum, shown in Fig. 3, is very congested and exhibits a total of 23 ^{1}H doublets, centered around the ^{1}H Larmor frequency, $\nu_H = 129.14$ MHz. For convenience, the frequency axis in the ^{1}H ENDOR and TRIPLE spectra is given relative to ν_H, namely $\nu_{RF} - \nu_H$. The 2D ^{1}H–^{1}H correlation spectrum, shown in Fig. 4a, allows a straightforward grouping of the ENDOR lines according to their respective centers and M_S manifolds by following the connectivities of each signal. For example a comparison with Fig. 1c shows that peaks connected with single and double dotted lines represent signal that belong to different M_S manifolds of one center, whereas the peaks connected with single and double dashed lines belong to different M_S manifolds of a second center. As there are no correlations between dashed- and dotted-marked peaks, they are assigned to different centers.

The analysis of the 2D spectrum revealed the presence of four sets of peaks (two different sites with two M_S manifolds in each) with correlations among them but not between them. Fifteen doublets were assigned to center I and 8 to center II. Out of the 15 protons of center I, 7 have a hyperfine coupling with the same sign and 8 with the opposite sign. In center II, 4 protons have the same sign and 4 the opposite sign. The ^{1}H peaks in the ENDOR spectrum depicted in Fig. 3a marked by open and solid symbols represent centers I and II, respectively, whereas triangles and circles are used to distinguish lines belonging different manifolds. The relative signs and magnitudes of the ^{1}H hyperfine couplings, a_i, of all these protons were used to simulate the ENDOR spectrum shown in the bottom of Fig. 3, and the 2D difference TRIPLE spectrum shown in Fig. 4b. The agreement between the experimental and calculated spectra is very good. The contour level cut off was set well above the noise level therefore some peaks are missing from the experimental spectra.

The ENDOR signals of the ^{2}H ($I = 1$), ^{14}N ($I = 1$), and

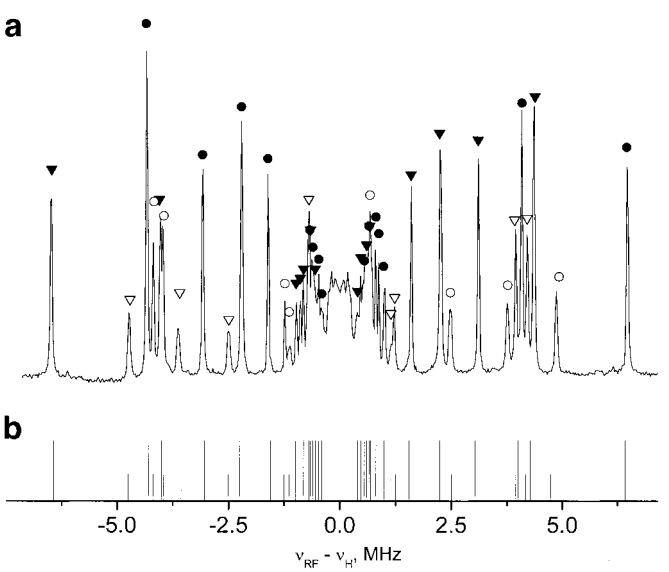

FIG. 3. (a) The W-band ^{1}H Davies ENDOR spectrum of a Cu–His crystal ($t_{MW} = 0.2/0.1/0.2$ μs, $\tau = 0.35$ μs, $t_{RF} = 25$ μs, $T = 5$ K, $B_0 = 3.0335$ T). Solid circles represent all the lines belonging to the $M_S = \frac{1}{2}$ manifold of center I, whereas the solid triangles label the lines of the other M_S manifold ($M_S = -\frac{1}{2}$). Similarly, empty circles and triangles label the lines belonging to center II. (b) Simulated ENDOR "stick"-spectrum (lines originating from different centers are depicted by sticks with different heights).

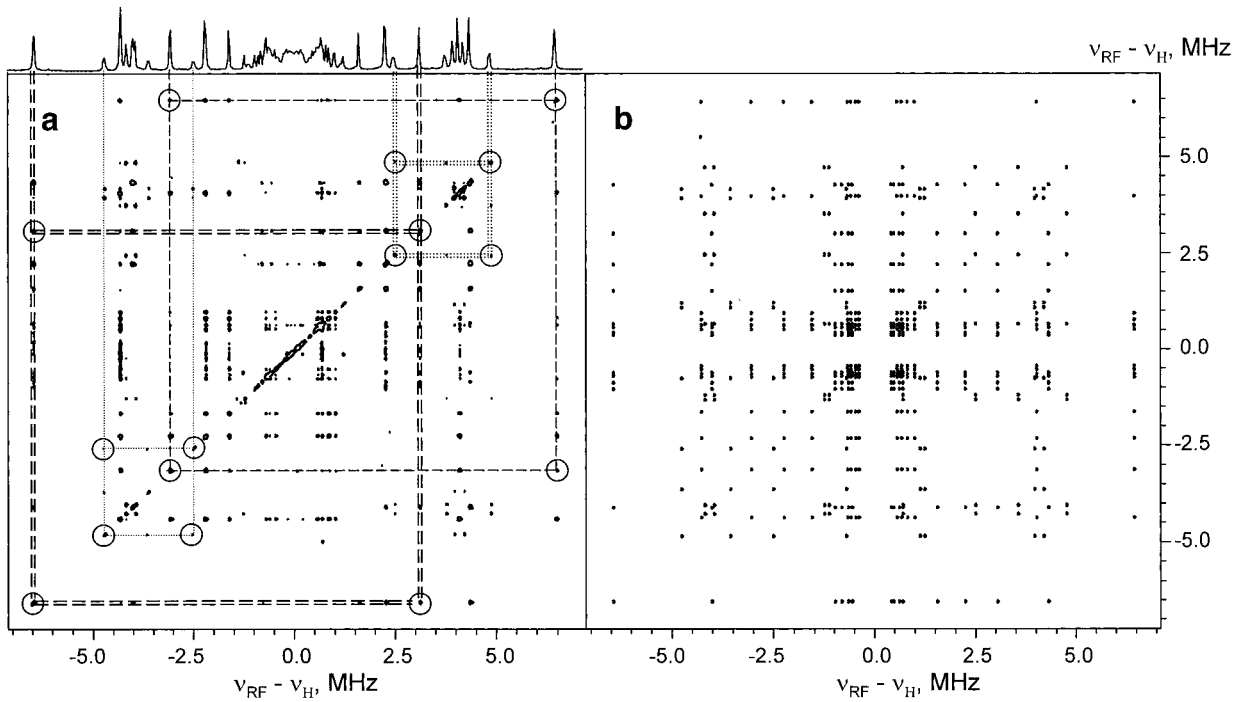

FIG. 4. (a) The experimental W-band 2D ^{1}H-^{1}H correlation difference TRIPLE spectrum of a Cu–His crystal (t_{MW} = 0.2/0.1/0.2 μs, τ = 0.35 μs, t_{RF} = 25/25 μs, T = 5 K, B_0 = 3.0335 T). For simplicity the contour level was chosen well above the noise level. Circles are drawn around correlation peaks of interest (see text). (b) The simulated ^{1}H-^{1}H correlation difference TRIPLE spectrum.

^{35}Cl ($I = \frac{3}{2}$) nuclei appear in the 1–27 MHz range, as shown in the ENDOR spectrum depicted in Fig. 5. All these are quadrupolar nuclei and the first-order expressions for their ENDOR frequencies is given by (*32*)

$$\nu_{i,M_I \to M_I+1} = \left| -\nu_I + M_S a_i + \frac{3}{2} Q_i (2M_I + 1) \right|, \qquad [2]$$

where Q_i is the element of the quadrupole coupling tensor for the respective orientation for nucleus i. This yields, for $\nu_I > |a_i|$, $|Q_i|$, symmetric doublets centered around ν_I. The frequency ranges of the weakly coupled remote ^{14}N and ^{2}H nuclei are indicated on the spectrum, where doublets symmetrically located about ν_N = 9.33 MHz and $\nu_{^2H}$ = 20 MHz are easily detected.

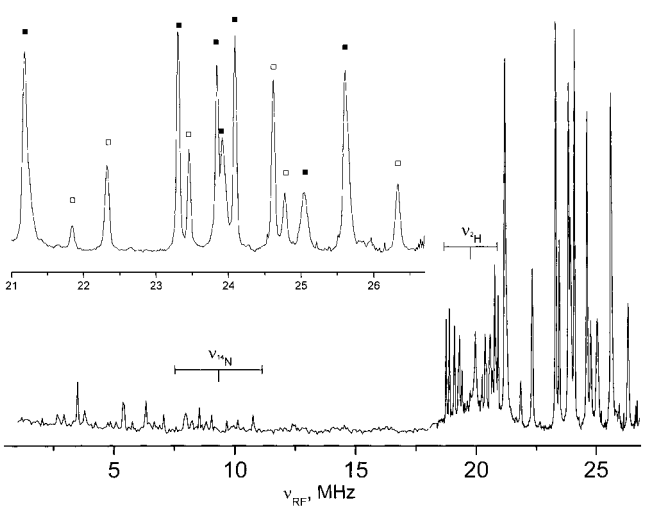

FIG. 5. The W-band Davies ENDOR spectrum of a Cu–His crystal in the ^{14}N, ^{35}Cl, and ^{2}H frequency range. The inset shows the upper frequency region of the spectrum (t_{MW} = 0.2/0.1/0.2 μs, τ = 0.35 μs, t_{RF} = 25 μs, T = 5 K, B_0 = 3.0335 T). The regions of weakly coupled ^{14}N and ^{2}H nuclei are indicated on the figure. The empty and solid squares label the peaks corresponding to the same M_S manifold in the two different centers, respectively.

The strongly coupled ^{14}N and ^{35}Cl nuclei appear as two groups of lines, one in the 20–27 MHz region and the other in the 2–7 MHz region, corresponding to the two different M_S manifolds. The intensities of the peaks in the high frequency region is significantly higher due to the hyperfine enhancement effect (*32*), which for the hyperfine values noted below is significant even at 3 T. The Larmor frequencies of ^{14}N and ^{35}Cl at 3.0335 T are quite close (9.33 and 12.66 MHz, respectively) and their hyperfine couplings are large and of the same order of magnitude (N_1: A_{xx}, A_{yy}, A_{zz} = 37.7, 29.3, 28.5 MHz, N_2: A_{xx}, A_{yy}, A_{zz} = 39.24, 25.92, 25.42 MHz, ^{35}Cl: A_{xx}, A_{yy}, A_{zz} = 63.1, 21.03, 18.48 MHz (*30*)). Consequently, their signals appear in the same frequency range also at W-band, leading to difficulties in differentiating the ^{14}N and ^{35}Cl peaks. Moreover, the peaks in the low frequency region originate from nuclei experiencing a small effective field and due to their

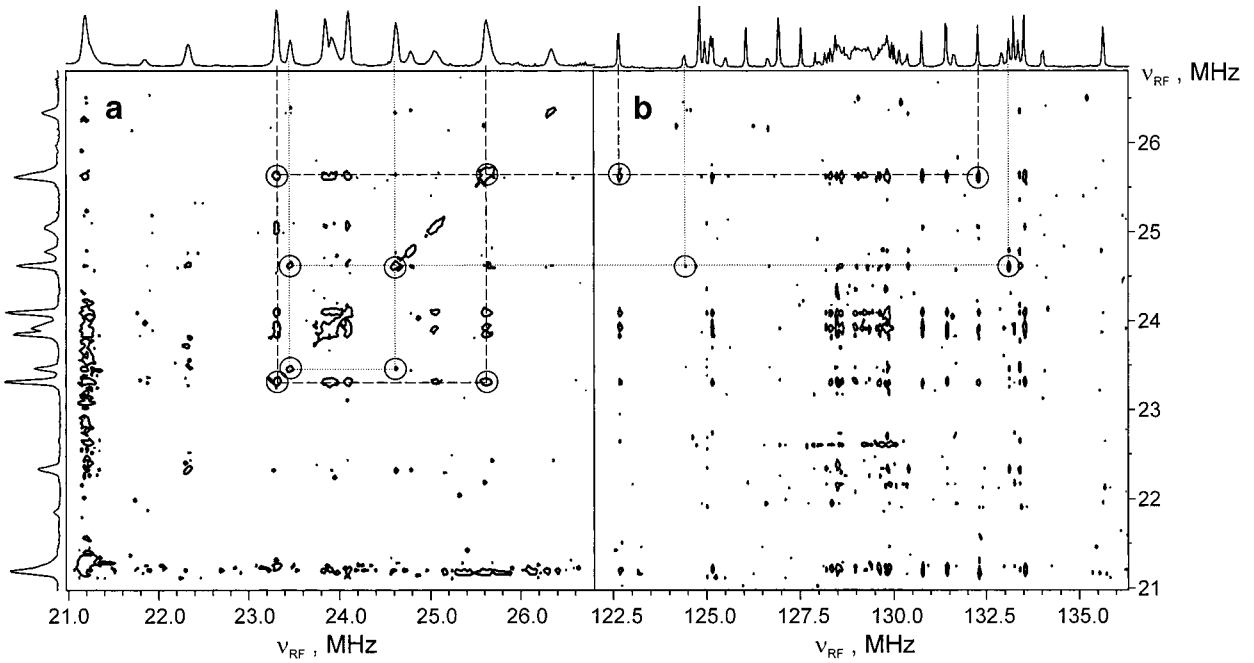

FIG. 6. (a) The 2D $^{14}N/^{35}Cl$–$^{14}N/^{35}Cl$ correlation difference TRIPLE spectrum of a Cu–His crystal (t_{MW} = 0.2/0.1/0.2 μs, τ = 0.35 μs, t_{RF} = 23/23 μs, T = 5 K, B_0 = 3.0335 T). (b) ^{1}H–$^{14}N/^{35}Cl$ correlation difference TRIPLE spectrum recorded with the same conditions as in (a) but t_{RF} = 25/23 μs for the ^{1}H and $^{14}N/^{35}Cl$ frequency ranges, respectively. Circles are drawn around correlation peaks of interest.

significant quadrupole interaction the ENDOR frequencies may deviate significantly from the first-order expressions, given in Eq. [2], usually used for their identification.

The 2D difference TRIPLE spectrum in the 21–27 MHz region, presented in Fig. 6a shows that the 13 lines observed in this region could be separated into the two mutually uncorrelated groups of 7 and 6 lines, which correspond to the two different centers, I′ and II′. Dashed and dotted lines show connectivities between selected lines of these groups. Since all lines that belong to one center exhibit correlations within this range it is concluded that they originate from hyperfine couplings with the same signs, in agreement with Ref. (*30*). The absolute sign of the strongly coupled $^{14}N/^{35}Cl$ hyperfine constants has been reported to be positive (*30*) and therefore the $^{14}N/^{35}Cl$ lines in the 21–27 MHz range correspond to the $M_S = -\frac{1}{2}$ manifold. In Fig. 5 ENDOR lines that belong to different groups are marked with solid (center I′) and empty (center II′) squares.

Through the ^{1}H–^{1}H and $^{14}N/^{35}Cl$–$^{14}N/^{35}Cl$ 2D TRIPLE experiments we assigned the protons signals to two centers, I, II, and the $^{14}N/^{35}Cl$ signals to the centers I′ and II′. The remaining problem is which ^{1}H and $^{14}N/^{35}Cl$ groups belong to the same center, (I, I′; II, II′) or (I, II′; II, I′). The right combination correlation can be determined by performing an hetero-nuclear correlation experiment.

The ^{1}H–$^{14}N/^{35}Cl$ TRIPLE spectrum, presented in Fig. 6b, was obtained by scanning RF_2 from 21 to 27 MHz and RF_1 from 135 to 155 MHz. Since the $^{14}N/^{35}Cl$ lines belong to one manifold, the positions of the heteronuclear correlation peaks will depend on the manifold in which the ^{1}H transitions take place. If the manifold is the same as that of the $^{14}N/^{35}Cl$ transition, peaks will appear at $RF_1 > \nu_H$, otherwise it will show at $RF_1 < \nu_H$. Following the correlations between selected peaks of group I (^{1}H) and group I′ ($^{14}N/^{35}Cl$), indicated by dashed lines in Figs. 6a, b, we conclude that (i) groups I and I′, and II and II′, belong to the same center and (ii) proton lines marked by solid triangles in Fig. 3 originate from the $M_S = -\frac{1}{2}$ manifold and those marked by solid circles are from the $M_S = +\frac{1}{2}$ manifold. The same procedure was applied to groups II and II′ (dotted lines in Figs. 6a and 6b). Accordingly, in center I, 8 ^{1}H nuclei have positive hyperfine couplings and 7 ^{1}H nuclei have negative couplings. In site II, 4 protons have positive couplings and 4 negative couplings. The assignments of all signals to their centers and M_S manifolds are summarized in Table 1, according to the labels used in Figs. 3–6.

TABLE 1
A Summary of the Symbols Used to Label the Assigned Peaks in Figs. 3–6

	^{1}H		$^{14}N/^{35}Cl$
Site	$M_S = \frac{1}{2}$	$M_S = -\frac{1}{2}$	$M_S = -\frac{1}{2}$
I	●	▼	■
II	○	▽	□

SUMMARY AND CONCLUSIONS

The extension of the 1D TRIPLE experiment to 2D considerably simplifies the assignment of congested ENDOR spectra and allows straight forward differentiation between ENDOR peaks belonging to different paramagnetic centers and M_S manifolds. Carrying out the experiment at high fields has the additional advantage that different types of nuclei, are well separated. The experiment was demonstrated on a crystal of Cu^{2+} l-doped histidine where homonuclear, ^{1}H–^{1}H and ^{14}N/^{35}Cl–^{14}N/^{35}Cl and heteronuclear ^{1}H–^{14}N/^{35}Cl correlations were obtained.

Based on the recent development of high frequency ENDOR which is highly sensitive to size limited samples, it is expected that more single crystal studies on proteins and other size limited crystals will become plausible and the 2D TRIPLE experiment will be very useful for spectral editing and assignment. In principle, the 2D TRIPLE experiment should be very useful also for orientationally disordered systems, provided that the number of coupled nuclei is relatively small. It can be useful in determining whether features in a powder spectrum indicate the presence of different nuclei or are merely due to singularities of the powder pattern attributed to the same nucleus. This is particularly important in orientation selective experiments where the shape of powder pattern is not known *a priori*. Furthermore, the correlation patterns observed should provide the relative orientations of the hyperfine interaction of the nuclei involved.

ACKNOWLEDGMENT

This research was supported by the DFG Schwerpunkt program "High field EPR in Physics, Chemistry and Biology." DG thanks P. Höfer for helpful discussions during her visit to Bruker.

REFERENCES

1. Y. S. Lebedev, Modern pulsed and continuous-wave electron spin resonance (L. Kevan and M. K. Bowman, Eds.), pp. 365–404, Wiley, New York (1990).
2. Y. S. Lebedev, Very-high-field EPR and its applications, *Appl. Magn. Reson.* **7,** 339–362 (1994).
3. K. A. Earle, D. E. Budil, and J. H. Freed, *in* "Advances in Magnetic and Optical Resonance" (W. S. Warren, Ed.), Vol. 19, pp. 253–323 (1996).
4. J. Disselhorst, H. Vandermeer, O. Poluektov, and J. Schmidt, A pulsed EPR and ENDOR spectrometer operating at 95 GHz, *J. Magn. Reson.* **115,** 183–188 (1995).
5. T. Prisner, M. Rohrer, and K. Möbius, Pulsed 95 GHz high-field EPR heterodyne spectrometer with high spectral and time resolution, *Appl. Magn. Reson.* **7,** 167–183 (1994).
6. I. Gromov, V. Krymov, P. Manikandan, D. Arieli, and D. Goldfarb, A W-band pulsed ENDOR spectrometer: Setup and application to transition metal centers, *J. Magn. Res.* **139,** 8–17 (1999).
7. M. Bennati, C. Farrar, J. Bryant, S. Inati, V. Weis, G. Gerfen, P. Riggs-Gelasco, J. Stubbe, and R. Griffin, Pulsed electron-nuclear double resonance (ENDOR) at 140 GHz, *J. Magn. Reson.* **138,** 232–243 (1999).
8. M. T. Bennebroek, O. G. Poluektov, A. J. Zakrzewski, P. G. Baranov, and J. Schmidt, Structure of the intrinsic shallow electron center in AgCl studied by pulsed electron nuclear double resonance spectroscopy at 95 GHz, *Phys. Rev. Lett.* **74,** 442–445 (1995).
9. J. W. A. Coremans, M. V. Gastel, O. G. Poluektov, E. J. J. Groenen, T. D. Glaauwen, G. V. Pouderoyen, G. W. Canters, H. Nar, C. Hamman, and H. Messerschmidt, An ENDOR and ESEEM study of the blue copper protein Azurin, *Chem. Phys. Lett.* **235,** 202–210 (1995).
10. D. Goldfarb, K. G. Strohmaier, D. E. W. Vaughan, H. Thomann, O. Poluektov, and J. Schmidt, Studies of framework iron in zeolites by pulsed ENDOR at 95 GHz, *J. Am. Chem. Soc.* **118,** 4665–4671 (1996).
11. M. M. Werst, C. E. Davoust, and B. M. Hoffman, Ligand spin density in blue copper proteins by Q-band ^{1}H and ^{14}N ENDOR spectroscopy, *J. Am. Chem. Soc.* **113,** 1533–1538 (1991).
12. V. Weis, M. Benatti, M. Rosay, J. A. Bryant, and R. G. Griffin, High field DNP and ENDOR with a novel multiple-frequency resonance structure, *J. Magn. Reson.* **140,** 293–299 (1999).
13. O. Burghaus, M. Plato, M. Rohrer, K. Möbius, F. MacMillan, and W. Lubitz, 3-mm high field EPR on semiquinone radical anions Q^{-} related to photosynthesis and on the primary donor P^{+} and acceptor Q_A^{+} in reaction centers of rhodobacter spheroids R-26, *J. Phys. Chem.* **97,** 7639–7649 (1993).
14. M. Rohrer, M. Plato, F. MacMillan, Y. Grishin, W. Lubitz, and K. Möbius, Orientation-selected 95 GHz high-field ENDOR spectroscopy of randomly oriented plastoquinone anion radicals, *J. Magn. Reson. A* **116,** 59–66 (1995).
15. P. Manikandan, R. Carmieli, T. Shane, A. J. Kalb (Gilboa), and D. Goldfarb, W-band ENDOR investigation of the manganese-binding site of concanavalin A: Determination of proton hyperfine couplings and their signs, *J. Am. Chem. Soc.* **122,** 3488–3494 (2000).
16. Y. S. Lebedev, A Specialist Periodical Report, "Electron Spin Resonance," Vol. 14, pp. 63–87 (1994).
17. D. Arieli, D. E. W. Vaughan, K. G. Strohmaier, and D. Goldfarb, High field ^{31}P ENDOR of $MnAlPO_4$-20: Direct evidence for framework substitution, *J. Am. Chem. Soc.* **121,** 6028–6032 (1999).
18. D. Goldfarb, Pulsed electron spin resonance techniques, *in* "Spectroscopy of Transition Metal Ions on Surfaces" (Bert M. Weckhuysen, P. V. D. Voort, and G. Catana, Eds.), pp. 93–134, Leuven University Press, Belgium (2000).
19. P. Höfer, A. Grupp, H. Nebenführ, and M. Mehring, Hyperfine sublevel correlation (HYSCORE) spectroscopy: A 2D ESR investigation of the squaric acid radical, *Chem. Phys. Lett.* **132,** 279–282 (1986).
20. D. Goldfarb, V. Kofman, J. Libman, A. Shanzer, R. Rahmatouline, V. Doorslaer, and A. Schweiger, Double nuclear coherence transfer (DONUT)-HYSCORE—A new tool for the assignment of nuclear frequencies, *J. Am. Chem. Soc.* **120,** 7020–7029 (1998).
21. G. Jeschke and A. Schweiger, Time-domain chirp electron nuclear double resonance spectroscopy in one and two dimensions, *J. Chem. Phys.* **103,** 8329–8337 (1995).
22. G. Jeschke and A. Schweiger, Hyperfine-correlated electron-nuclear double resonance spectroscopy, *Chem. Phys. Lett.* **246,** 431–438 (1995).
23. G. Bar, A. Pöppl, S. Vega, and D. Goldfarb, Two-dimensional ENDOR-ESEEM correlation spectroscopy, *J. Magn. Reson.* **145,** 115–124 (2000).

24. R. Cook and D. H. Whiffen, Relative signs of hyperfine coupling constants by a double ENDOR experiment, *Proc. Phys. Soc.* **84,** 845–848 (1964).

25. B. Biehl, M. Plato, and K. Möbius, General TRIPLE resonance on free radicals in solution. Determination of relative signs of isotropic hyperfine coupling constants, *J. Chem. Phys.* **63,** 3515–3522 (1975).

26. M. Mehring, P. Höfer, and A. Grupp, Pulsed electron nuclear double and triple resonance schemes, *Ber. Bunseges. Phys. Chem.* **91,** 1132–1137 (1987).

27. P. E. Doan, C. Fan, and B. M. Hoffman, Pulsed ^{1,2}H ENDOR and ^{2}H-^{2}H TRIPLE resonance of H-bonds and cysteinyl β-CH_2 of the *D. gigas Hydrogenase* [3Fe–4S]$^{+}$ Cluster, *J. Am. Chem. Soc.* **116,** 1033–1041 (1994).

28. M. Hubrich, G. G. Maresch, and H. W. Spiess, Application of pulsed ENDOR to the study of radicals in a liquid-crystalline copolymer, *J. Magn. Reson. A* **113,** 177–184 (1995).

29. R. Hirasawa and H. Kon, Electron paramagnetic resonance and polarized absorption spectra of Cu(II)-doped single crystal of L-histidine hydrochloride monohydrate, *J. Chem. Phys.* **56,** 4467–4474 (1972).

30. C. McDowell, A. Naito, D. Sastry, Y. Cui, K. Sha, and S. Yu, Ligand ENDOR study of Cu(II)-doped L-histidine deuterochloride monodeuterohydrate single crystals at 4.2 K, *J. Mol. Struct.* **195,** 361–381 (1989).

31. J. J. Shane, P. A. A. W. V. der Heijden, E. J. Reijerse, and E. de Boer, An ESEEM investigation of single crystals and powders of copper-doped L-histidine hydrochloride monohydrate, *Appl. Magn. Reson.* **6,** 427–454 (1994).

32. H. Kurreck, B. Kirste, and W. Lubitz, "Electron Nuclear Double Resonance Spectroscopy of Radicals in Solution," Chap. 3, VCH, Weinheim/New York (1988).